Magnetic impurities in HNb_2O_5

2001 J. Phys.: Condens. Matter 13 11017

(http://iopscience.iop.org/0953-8984/13/48/326)

INSTITUTE OF PHYSICS PUBLISHING JOURNAL OF PHYSICS: CONDENSED MATTER

J. Phys.: Condens. Matter **13** (2001) 11017–11025 PII: S0953-8984(01)24723-7

Magnetic impurities in HNb_2O_5

Osvaldo F Schilling[1] **and Luis Ghivelder**[2]

[1] Departamento de Física, Universidade Federal de Santa Catarina, Campus Universitário, 88040-900, Florianópolis, SC, Brazil
[2] Instituto de Física, Universidade Federal do Rio de Janeiro, CP 68528, 21945-970, Rio de Janeiro, RJ, Brazil

E-mail: osvaldof@mbox1.ufsc.br and luisghiv@if.ufrj.br

Received 10 May 2001, in final form 28 August 2001
Published 16 November 2001
Online at stacks.iop.org/JPhysCM/13/11017

Abstract

Cu, Fe, Gd and Nd dopants were added to HNb_2O_5 in a range of concentrations to investigate the influence on the magnetic properties. The dopants fill the vacant sites in the channels along the b axis of the structure. Magnetic moments tend to remain localized in the dopants. AC susceptibility measurements display low temperature undulations associated with short range magnetic correlations within small clusters (of two or three ions) of dopants. Glauber spin-flip kinetics for Ising spin rings can be applied to these data. Although the magnetic behaviour is mostly Curie–Weiss above 20 K, the susceptibility data display a temperature-independent residual paramagnetic signal. We attribute this signal to Van Vleck orbital paramagnetism associated with bonding–antibonding transitions within Nb^{4+} or Cu^{2+} spin-paired dimers.

1. Introduction

The magnetic interactions between localized or itinerant electrons in oxides are associated with a variety of physically and technologically interesting phenomena. Colossal magnetoresistance, spin-Peierls transitions, high-temperature superconductivity in cuprates and spin-glass transitions are among these phenomena. The role played by dopants in perovskites and other kinds of oxide structures is particularly relevant to the magneto-transport properties of such compounds. For instance, colossal magnetoresistance is deeply associated with the influence of rare-earth and alkaline-earth dopants upon superexchange interactions between Mn ions in perovskites [1]. These ions affect the bond angles between Mn and O in the structure in such a way that the control of dopant concentration actually determines the sign of the exchange integrals, and even whether or not the metal–insulator transition takes place.

Following these lines, we have undertaken a study of the effects of transition metal (TM) and rare-earth (RE) metal additions to the magnetic properties of HNb_2O_5 (hereafter

referred to also as the H-phase). The H-phase structure is a semiconductor which contains channels of empty octahedral and tetrahedral sites parallel to the monoclinic b axis. Detailed transmission electron microscopy studies demonstrated that added dopants tend to occupy such sites and form quasi-one-dimensional chains [2, 3]. The magnetic properties measured in doped H-phase are related to magnetic moments localized on the dopants rather than the matrix, which is mostly non-magnetic since it is formed by d^0 Nb^{5+} ions (and also by spin-paired d^1 Nb^{4+} ions when reduced to Nb_2O_{5-x}). The present paper complements our previous study on the subject, hereafter referred to as part I [4]. In part I we carried out dc and ac magnetic susceptibility measurements in an Fe-doped sample of H-phase (here called sample Fe-I), which were consistent with the formation of one-dimensional arrays of Fe^{2+} along the b-axis channels in the structure. In the present paper we extend the investigation to include Cu, Gd and Nd as dopants at several different concentrations. Once again we obtained evidence of the formation of correlated localized moments distributed along the channels. The variation of dopant content provides further information. The susceptibility data display a temperature-independent residual paramagnetic component which saturates at a constant level for the highest dopant concentrations tested. We tentatively attribute such residual susceptibility to a Van Vleck orbital paramagnetism associated with bonding–antibonding transitions within paired electrons or holes localized along the channels.

2. Experimental methods

The samples were prepared by mixing and heat treating chemical grade Fe_2O_3, (or Gd_2O_3, Nd_2O_3 or CuO) and NbO_2 powders for 24 h at 1050 °C, to obtain the atomic proportions shown in table 1. The objective was to cover a range of spacings between dopants along the channels of the structure, varying from very sparse to about one dopant per cell (one unit cell contains 28 Nb atoms) and check the effects on the magnetic properties. The samples were analysed by x-ray diffraction which displayed the spectra of the H-phase only. Measurements of dc magnetization and ac susceptibility were carried out in a commercial magnetometer (Quantum Design PPMS). The ac measurements were taken with an exciting field of 10 Oe and frequency of 1 kHz . The measurements covered temperatures down to 1.8 K and dc magnetic fields up to 9 T.

Table 1. Overall information about sample compositions, including the magnetic moment per ion obtained from magnetization measurements.

Sample	Composition (dopants per unit cell)	Dopant valence (from the number of Bohr magnetons)	n_0	Number of Bohr magnetons per dopant	Number of Bohr magnetons per dopant (expected)
Fe-I	0.33	+2	0.66	5.35	5.1–5.3
Fe-II	1	+2	2	5	5.1–5.3
Cu-I	1.6	*	3.2	1.36	1.73–1.9
Cu-b	0.4	+2	0.8	1.93	1.73–1.9
Cu-d	0.11	+2	0.22	2.2	1.73–1.9
Gd-a	0.67	+3	2	7.6	7.9
Gd-b	0.2	+3	0.6	7.6	7.9
Nd-a	0.5	+2	1	2.3	2.68
Nd-b	0.2	+2	0.4	2.6	2.68

* Cu valence is +2 but spin-paired ions make the measured moment decrease.

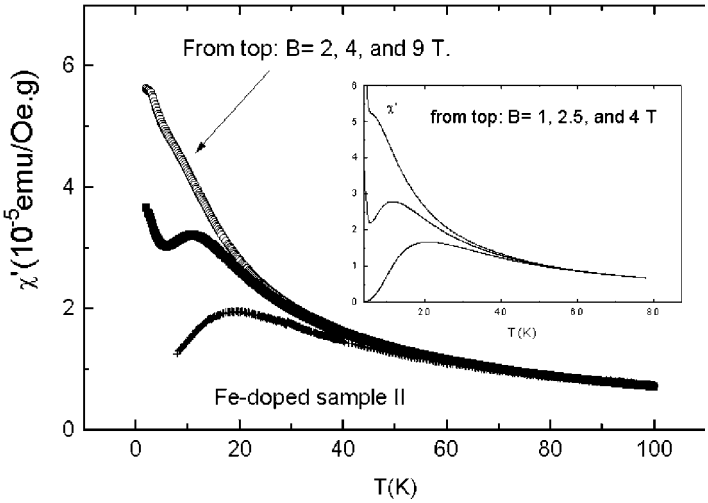

Figure 1. Susceptibility measurements taken for the Fe-II sample. The inset shows simulations for the superposition of five dimers (with $J = 4$ K) and one trimer (with $J_{12} = 4$ K, $J_{23} = 4$ K and $J_{13} = -4$ K between neighbouring atoms 1, 2 and 3 in a ring). We adopted the product $g\sigma = 5$ (= number of Bohr magnetons per dopant) in the equations of the model in part I [4].

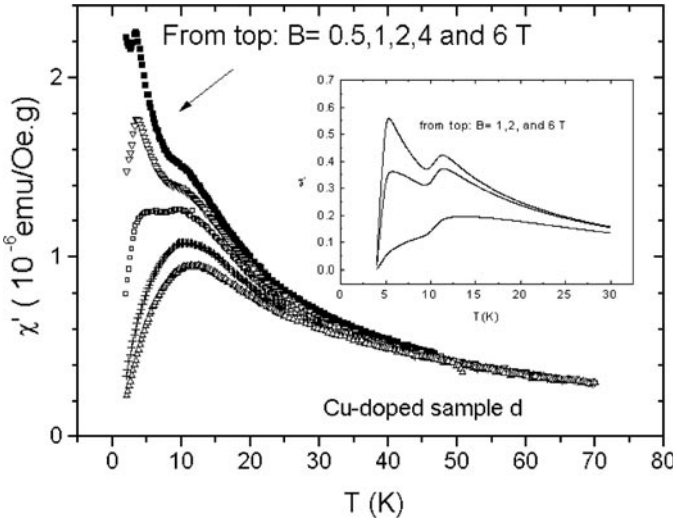

Figure 2. Susceptibility measurements taken for the Cu-d sample. The inset shows simulations for the superposition of 70% of dimers with $J = 30$ and 30% with $J = 70$ K. We adopted the product $g\sigma = 2$ in the equations of the model in part I [4].

3. Experimental results

Figures 1–5 show ac susceptibility measurements for Fe-, Cu-, Gd- and Nd-doped samples. They are similar to the Fe-I sample results in part I. The behaviour is mostly Curie–Weiss above 20 K but a residual susceptibility remains at high temperature. The data measured for

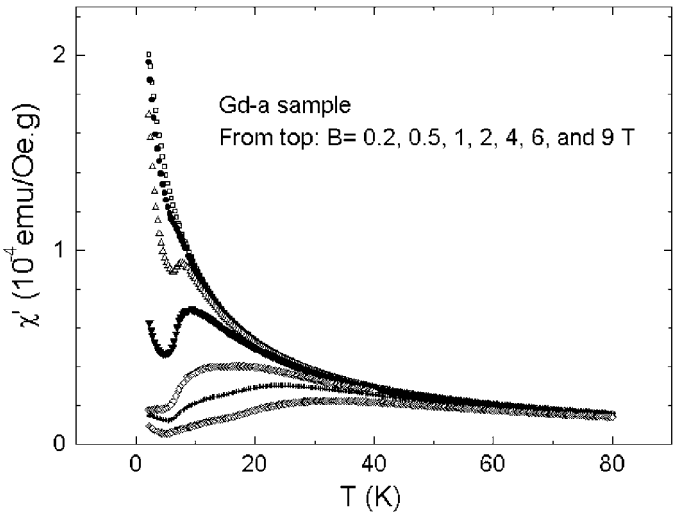

Figure 3. Susceptibility measurements taken for the Gd-a sample.

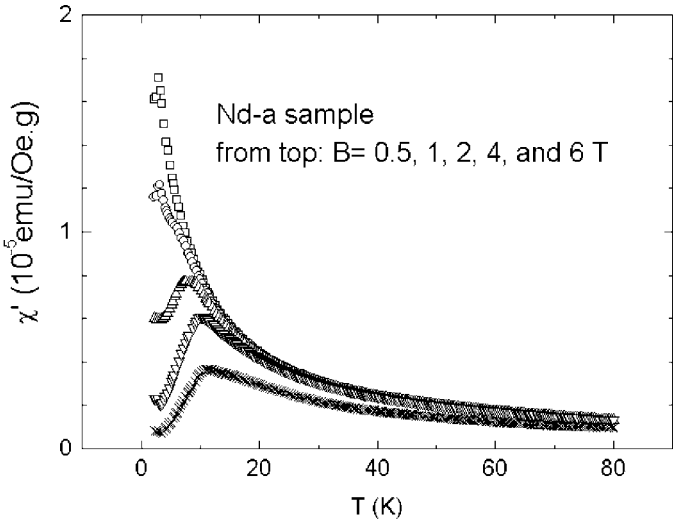

Figure 4. Susceptibility measurements taken for the Nd-a sample.

0.2 or 0.5 T dc field for each sample were fitted to a modified Curie–Weiss law $\chi = C/(T-\theta) + \chi_0$. The modified Curie–Weiss law fits perfectly well to each set of data, and the uncertainty estimated for each value of χ_0 obtained from the fits is less than 5%. We also took M versus H measurements at constant temperature (not shown) to complement the susceptibility data and obtained the magnetic moment per dopant and dopant valence in each sample. The overall data are displayed in table 1. The parameter χ_0 is plotted in figure 6 against the parameter $n_0 =$ (dopant valence) $\times$ (number of dopants per unit cell). This latter parameter is used as a measure of the total number of electrons donated per dopant per unit cell. The data points in figure 6 are apparently divided into two groups, each one of them converging to a different saturation value of χ_0 for $n_0 > 1$.

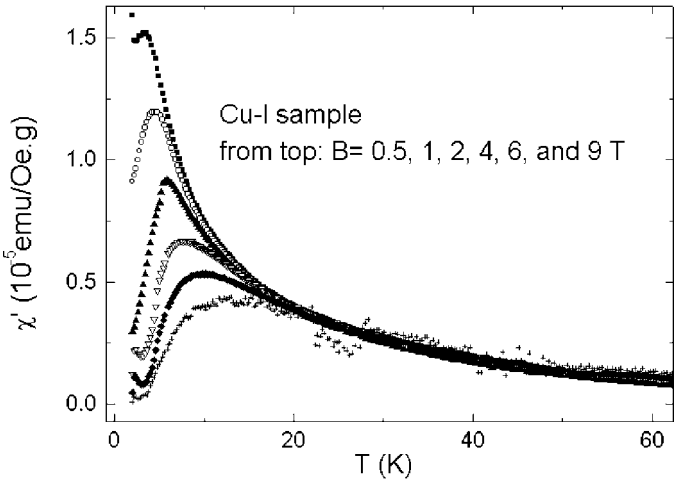

Figure 5. Susceptibility measurements taken for the Cu-I sample.

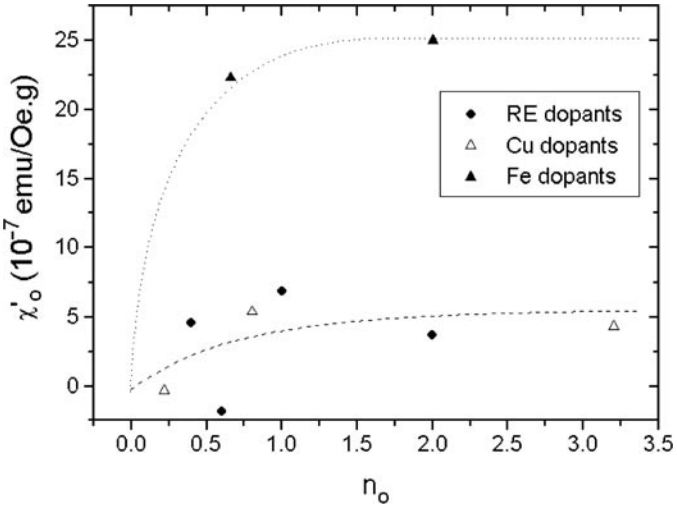

Figure 6. The residual susceptibility plotted against the parameter n_0. The dashed lines are guides for the eye. The uncertainty in each point is about the size of the symbols used in the plot.

4. Analysis

The similarity between the low-temperature undulations in the ac susceptibility curves is indicative of their common origin for all samples, i.e., correlations between neighbouring dopants along channels, involving two (dimers), and possibly three ions (trimers) or more, forming what we might call 'rings'. In part I we developed a model to apply Glauber's one-step spin-flip dynamics to calculate the ac susceptibility of short rings of $1/2$-spin moments, coupled by nearest-neighbour interactions [4–6]. The experimental results may be reproduced by assuming that dimers (and trimers, etc) having different coupling constants J exist along the channels. The rings may be characterized by the exchange coupling constant J between their spins (see theory and notation in part I). The inset in figure 1 displays theoretical susceptibility

curves for a mixture of dimers and trimers that reproduces the data for sample Fe-II. Trimers were included since at high concentrations of dopants correlations involving spins from more than two dopants should be expected. The simulations are calculated for the superposition of five dimers (with $J = 4$ K) and one trimer, with $J_{12} = 4$ K, $J_{23} = 4$ K and $J_{13} = -4$ K between neighbouring atoms in a ring. The inset in figure 2 shows a similar simulation for the lightly doped Cu-d sample. The theoretical curve is calculated for the superposition of the effects of two kinds of dimers, with $J = 30$ K and 70 K, and assuming that 70% of the dimers have the weaker coupling $J = 30$ K. The assumption that most dimers have low J should be consistent with the large average spacing between dopants in the Cu-d sample. Figures 3 and 4 for the Gd-a and Nd-a samples display single peaks situated on top of a Curie–Weiss-like curve. This suggests the presence of isolated ions as well as dimers of a single kind, characterized by one value of J only. This would be consistent with the large ionic radii of the RE ions and their short-range f-shell orbitals, which would severely restrict the number of possible configurations for dimers as well as the magnitude of J. At higher concentration trimers and other configurations should also be accounted for. What is expected is that at high concentrations the superposition of the effects of different dimers, trimers, etc, will smear out the undulations and produce a single maximum. This is consistent with the susceptibility measured for sample Cu-I in figure 5 which is highly doped with 1.6 Cu per unit cell. The utility of the theoretical curves is to show that the measured ac susceptibility is consistent with the expected 'ring' configurations. It must be pointed out that the values of J are not unique since the theoretical curves depend also on the relative concentration of different kinds of clusters of dopants, which is used as another fitting parameter. It is important to discuss why clusters of dopants should be formed. There must be strong electrostatic and elastic interactions between the dopants. All these interactions lead to dopant clustering at the high temperatures (1050 °C) adopted during sample heat treatment. Such cluster concentrations are eventually expected to stabilize in a configuration of minimum overall energy.

It is interesting to note that the experimental data, taken for a wide range of values of total spin per ion, follow the Glauber kinetics for Ising spin lines quite closely. This suggests that anisotropy effects may severely limit the number of different states available for spin flips accessible by the ac susceptibility technique in such a way that the two-state kinetics of Ising spins still succeeds in reproducing the data (the effect of anisotropy on spin-orbit and crystal-field splitting is discussed in [7]).

Figure 7 shows a schematic band structure for doped HNb_2O_5. There is no detailed calculation of its band structure in the literature. However, band structure information is needed to evaluate whether moments on certain dopants should be localized or itinerant. For such purpose the ability to estimate the relative positions of valence and conduction bands compared to the dopants' energy levels is most important. To draw the band scheme shown in figure 7 we follow the previous work of Goodenough [8] and Harrison [9]. The tight-binding calculations of Harrison [9] for perovskites and other families of oxides are mainly based upon the assumption that the *relative* values of neutral atom orbital eigenenergies are maintained when the atoms are joined together to form a predominantly ionic solid. Therefore, neutral atom orbital energies are usually adopted in band construction. The main argument in support of this assumption is that when the neutral atoms exchange charge and condense to form the solid the difference in local Madelung potential energies between cation and anion sites is approximately cancelled by the potential energy involved in the charge transfer from cation to anion. The net difference between the cation and anion orbital energies ends up of the same order of magnitude as the difference between the neutral atoms' orbital eigenenergies, so that these latter quantities are eventually adopted in approximate band calculations (see [10] for a simple discussion about this matter). In the present case, the valence band should be mainly

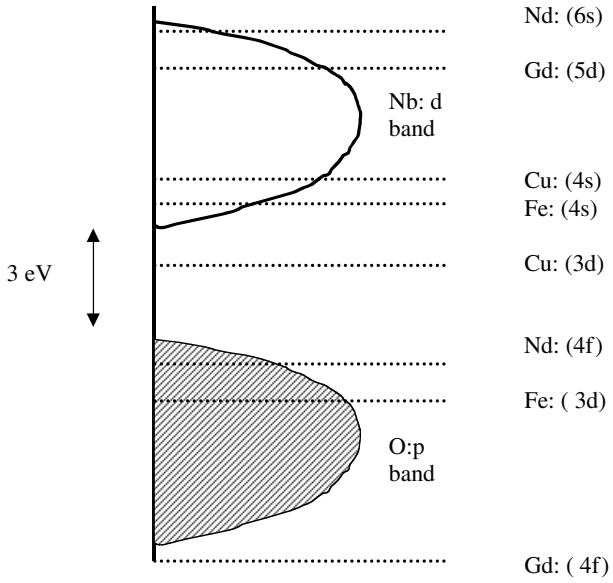

Figure 7. Schematic band structure of doped HNb_2O_5 including the neutral atoms relevant energy levels [11].

O: 2p in character and the conduction band mainly Nb: 4d. Such bands should be centred on the corresponding neutral atom orbital energies, with bandwidths of about 4–5 eV [9]. Following similar arguments, the dopant energy levels are taken as the same as the corresponding atomic orbital energies. Again it must be stressed that the *relative positions* of these bands and energy levels are more relevant for the analysis than their absolute values. For this reason there is no numerical scale indicated in figure 7, a procedure widely adopted by Goodenough [8] (the 3 eV energy gap is an experimental result). The neutral atom orbital energy values adopted are taken from the tables in the book by Herman and Skillman [11]. Other methods for estimating such energy diagrams exist. Torrance *et al* [12] adopt ionization energies for the gas-phase atoms added to the local Madelung potential energies to obtain energy levels for the solid instead of taking the neutral atom orbital eigenenergies. In that case the overall diagrams tend to display energy gaps that are too wide compared to reality. We believe that the diagram shown in figure 7 has the virtue of being consistent with the actual energy gap of 3 eV [13] observed between the oxygen p-band and the Nb d-band, provided we assume bandwidths of approximately 5 eV for both Nb d- and O p-bands.

We use this schematic energy level diagram to analyse the data in table 1 as well as the residual paramagnetic susceptibility shown in figure 6. The following analysis is possible:

(a) Nd cedes its s electrons to the Nb d-band, forming spin-paired Nb^{4+} ions. Spin-paired Nb^{4+} ions are reported to form bipolarons in reduced Nb_2O_{5-x} [14]. Nd 5d levels are empty and its 4f levels lie within the filled valence band, indicating that its four f electrons remain localized, which is consistent with the observed valence Nd^{2+}.

(b) Gd cedes its 6s and 5d electrons to Nb, in the same way as Nd does. The Gd 4f levels lie deep below the O p-band, which is consistent with the localization of its seven f electrons and the observed valence Gd^{3+}.

(c) The analysis for the Fe-doped sample II is similar to the one for Nd as far as the total moment is concerned. The observed valence Fe^{2+} is consistent with the positions of the energy levels.

(d) The magnetic moments on Cu vary substantially with concentration. The lightly doped samples Cu-b and d display about 2 Bohr magnetons per ion but the moment decreases for sample Cu-I. This would imply Cu^{2+} valence in samples b and d, and a mixture of Cu^{2+} and singlet paired ions in the highly doped sample I. The Cu 3d energy levels are in the middle of the energy gap. The valence +2 indicates that Cu donates one d electron to oxygen, which requires the presence of Nb vacancies: the lack of Nb ions opens holes in the O: 2p valence band to be filled by Cu electrons. Since all these samples display evidence for the presence of correlated spin pairs (dimers), the simplest explanation for the reduced valence appears to be that a substantial proportion of the Cu^{2+} ions in sample I pair antiferromagnetically into a singlet configuration, as in CuO[8]. Such AF pairs may exist in samples b and d also.

(e) The samples display a residual temperature-independent paramagnetic susceptibility that becomes independent of the number of electrons donated by the dopants beyond $n_0 \approx 1$ electron per unit cell (figure 6). By comparison with a similar result observed in $(Ti_{1-x}V_x)_2O_3$ (which contains paired Ti^{3+} d^1 ions [15]) we tentatively attribute this residual susceptibility to Van Vleck paramagnetism of localized moments in dimers formed either by Cu^{2+} ions (Cu-doped samples) or by Nb^{4+} ions (other samples). As discussed earlier, Nb^{4+} ions are formed by electron transfer from the 4s and 6s electrons of the dopants Fe, Nd and Gd. Electrons in neighbouring d^1 Nb^{4+} ions may thus occupy homopolar bonding and antibonding states separated by an energy δ. The Van Vleck susceptibility would be temperature independent and proportional to $1/\delta$. A similar interpretation may apply to coupling between holes in d^9 Cu^{2+} ions. The saturation of the value of the residual susceptibility for n_0 greater than 1 is probably the result of the saturation in the number of reduced Nb^{4+} or Cu^{2+} ions distributed along the channels. It seems unlikely that the structure will sustain more than one Nb^{4+} ion per unit cell along the channels [14]. Calculations carried out by one of the authors have shown that when the concentration of reduced cations reaches one cation per unit cell HNb_2O_5 transforms into $Nb_{53}O_{132}$ [16]. Therefore, it appears that saturation should actually be reached at dopant concentrations corresponding to one reduced cation per cell ($n_0 = 1$). This occurs for concentrations of about 0.33–0.5 dopant per cell, with each dopant donating two or three electrons. The data in figure 6 also show that the Fe-doped samples have a substantially greater value of χ_0 than the other samples, whose susceptibilities apparently saturate at a lower level. A quantitative interpretation of this result would require a more detailed investigation of the structural and energetic effects of each dopant ion, which is beyond the scope of this paper. Further addition of dopant ions may result in quasi-metallic behaviour, as reported for Nb_2O_{5-x} for $x > 0.05$ [17].

5. Conclusions

The ac susceptibity measured for Fe-, Cu-, Gd-, and Nd-doped HNb_2O_5 samples are consistent with the formation of dimers and possibly trimers of dopants along the channels, and the spin-flip kinetics can be described by the Glauber model applied to Ising spin chains. The valences observed for the Fe, Cu, Gd, and Nd ions are consistent with the positions of the corresponding energy levels relative to the conduction (Nb: 4d) and valence (O: 2p) bands of the H-phase compound. Fe, Nd, and Gd donate s and d electrons to Nb to form Nb^{4+} ions, which pair antiferromagnetically. Cu does not donate electrons to Nb, but the observed magnetic moments in Cu-doped samples are consistent with the presence of AF pairs of Cu^{2+} ions. The presence of such AF pairs is consistent with the measurement of a residual

Van Vleck paramagnetic susceptibility, which saturates for dopant concentrations such that one electron or hole per unit cell gets involved in pairing with particles in neighbouring cells.

Acknowledgments

This work was partially financed by the Brazilian Ministry of Science and Technology and by Conselho Nacional de Desenvolvimento Científico e Tecnológico, under the contract FAURGS/CNPq no 662187/1996–2. OFS wishes to thank Professor Paulo Pureur for the provision of laboratory facilities.

References

[1] Goodenough J B 1997 *J. Appl. Phys.* **81** 5330
[2] Anderson J S, Browne J M, Cheetham A K, von Dreele R, Hutchison J L, Lincoln F J, Bevan D J M and Straehle J 1973 *Nature* **243** 81
[3] Skarnulis A J, Iijima S and Cowley J M 1976 *Acta Crystallogr.* A **32** 799
[4] Schilling O F and Ghivelder L 2000 *J. Phys.: Condens. Matter* **12** 2825
[5] Reger J D and Binder K 1985 *Z. Phys.* B **60** 137
[6] Glauber R J 1963 *J. Math. Phys.* **4** 294
[7] Goodman B A and Raynor J B 1970 *Adv. Inorg. Chem. Radiochem.* **13** 135
[8] Goodenough J B 1971 *Prog. Solid State Chem.* **5** 145
[9] Harrison W A 1989 *Electronic Structure and the Properties of Solids* (New York: Dover)
[10] Sutton A P 1993 *Electronic Structure of Materials* (Oxford: Oxford University Press)
[11] Herman F and Skillman S 1963 *Atomic Structure Calculations* (New Jersey: Prentice-Hall)
[12] Torrance J B, Lacorre P, Asavaroengchai C and Metzger R M 1991 *Physica* C **182** 351
[13] Rüscher C H 1992 *Physica* C **200** 129
[14] Rüscher C H and Nygren M 1991 *J. Phys.: Condens. Matter* **3** 3997
[15] Dumas J, Schlenker C, Tholence J L and Tournier J L 1979 *Phys. Rev.* B **20** 3913
[16] Schilling O F 1986 *J. Phys. Chem. Solids* **47** 595
[17] Rüscher C, Salje E and Hussain A 1988 *J. Phys. C: Solid State Phys.* **21** 3737